GROUND-BASED TESTS OF A DIGITAL DISPLACEMENT HYDRAULIC TRANSMISSION FOR DISTRIBUTED PROPULSION

Niall Caldwell, niall.caldwell@flowcopter.com, Flowcopter Ltd. (UK)

Peter McCurry, peter.mccurry@flowcopter.com, Flowcopter Ltd. (UK)

Uwe Stein, uwe.stein@flowcopter.com, Flowcopter Ltd. (UK)

Duncan Menzies, duncan.menzies@flowcopter.com, Flowcopter Ltd. (UK)

Abstract

This paper progresses the concept of the Digital Displacement hydrostatic transmission as applied to hybrid multirotor UAVs and other applications of distributed propulsion. A summary of the concept is made and the simulation work done to date is described on the H380 UAV concept. A ground based test facility is described, and results are shown for steady state and transient rotor performance, with validation of the simulation model. Thermal performance is shown. An outlook for development towards flight testing is made.

1. INTRODUCTION

To extend flight times of electrically-powered multirotor UAV's, researchers have sought to replace or supplement the battery with a liquid-fueled internal combustion engine and electric series transmission, allowing 15 times more useful mechanical energy to be generated for each unit of weight [1].

In principle, an electric hybrid architecture allows the engine to be sized for the cruise power, rather than the peak power during takeoff, when the batteries can temporarily supplement the engine power. However, for rotorcraft requiring continuous hover duty, the engine must be rated for this continuous power, which is typically the peak power point. In this case there is little justification to include electrical energy storage, and the role of the electrical propulsion system reduces to that of a continuously-variable transmission with one input and multiple outputs.

It is commonly assumed in the aerospace field that electrical systems are the only viable option for such situations. Hydraulic systems are commonly used to couple a single prime mover to multiple variable-speed loads in applications such as excavators or combine harvesters, and indeed hydraulic systems are commonly applied to rotorcraft, but for actuation of rotor swashplates and landing gear, rather than propulsion. Hydraulic motors have the advantage of high specific power (as much as 16kW/kg), compact dimensions, tolerance of shocks and harsh environments, and low cost. However, traditional hydraulic systems suffer from poor energy efficiency, and control problems such as hysteresis, delay and non-linearity.

Recently, **Digital Displacement®** technology has emerged[4,5,6] as an alternative to traditional hydraulic systems. Advantages include improved energy efficiency, faster control response[3], lack of hysteresis, and the enabling of more efficient system architectures by the provision of multiple controllable fluid outputs[7]. In 2017, a patent application[8] was filed by Artemis Intelligent Power Ltd. describing the application of Digital Displacement to distributed propulsion for aircraft. This patent, and a license to the background technology, is now owned by Flowcopter Ltd, a company formed in the UK to commercialize the innovation.

In a previous paper[2] the Digital Displacement concept was introduced, and the design and expected performance of a proposed UAV based on the technology was predicted using a computer simulation model, which was described in detail.

The aim of this paper is to validate some of the core elements of this simulation model with data gathered from full-scale ground testing at the Flowcopter facility, with focus on the hydraulic system and rotor.

A summary of the system concept is given, and the expected features and performance are described of a UAV embodying it. The basic modelling equations are described, and the structure of a computer simulation is shown. A ground based test rig is described. Test results are shown of rotor and hydraulic system performance and under static and transient conditions, and compared to the simulation model.

2. SUMMARY OF SYSTEM CONCEPT

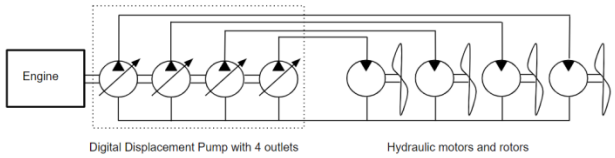

Figure 1: Basic concept of Digital Displacement transmission for a multirotor UAV

The basic concept of the transmission proposed for a quadcopter is shown above (Figure 1)

Briefly, the system comprises an aircraft engine, driving a Digital Displacement pump with four independently-controllable hydraulic outputs, each of which provides fluid to a hydraulic motor, driving a rotor. Compared to an equivalent electric transmission, it is expected to be 56% of the mass and 26% of the cost[2].

The digital hydraulic transmission is further described as part of an outline design of the "H380", a quadrotor UAV of maximum take-off weight 380kg, intended for offshore logistics, search and rescue, maritime patrol, agriculture, and other applications in harsh environments requiring a combination of continuous hover capability, and relatively long endurance and high payload capacity compared to equivalent battery-powered UAVs.

Figure 2: Visualization of the H380 concept

The basic parameters of the H380 are shown below:

Empty weight [kg]	230
Payload + fuel load [kg]	150
Max. take-off weight [kg]	380
Engine power pk./cont. [kW]	104 / 99
Number of rotors	4
Rotor diameter [m]	1.6

Figure 3: H380 basic parameters

The expected performance of the H380 is shown below, as detailed previously[2]

Payload [kg]	0	50
Hover Endurance [mins]	542	306
Flight Endurance [mins]	750	414
Speed at best endurance [km/h]	87.5	97.2
Range at best consumption [km]	1606	902
Speed at best consumption [km/h]	153.4	159.8

Figure 4: H380 expected range and endurance

The H380 is expected to reduce fuel consumption and CO2 emissions by 90% compared to a light twin-engined helicopter such as the Eurocopter EC135 while also exhibiting superior range and endurance.

A schematic of the proposed control system for the H380 is shown below.

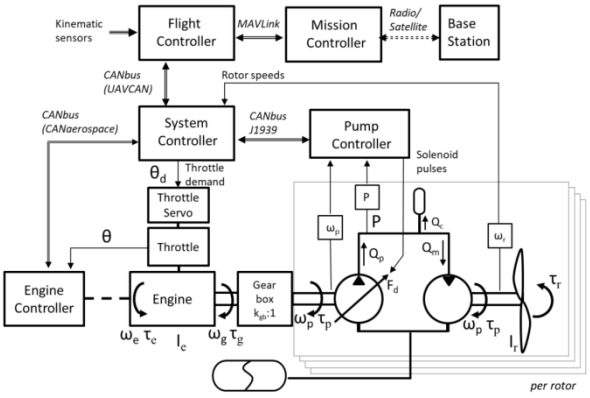

Figure 5: System schematic (showing only one pump outlet and associated rotor for clarity)

The control system was described in detail previously[2]. Briefly, the high-level control (mission and flight controller) is similar to battery-electric UAV's. Rotor speed demands are sent to a system controller, which is responsible to stabilize the engine speed via the throttle, and to control the rotor speed via the displacement command of each

pump outlet, subject to limit functions for the torque, pressure and engine speed.

3. MODELLING EQUATIONS OF THE PROPULSION SYSTEM

The equations are presented here for modelling the digital hydraulic propulsion system, comprising engine, gearbox, pump, motors and rotors.

The displacement of a hydraulic pump is the amount of fluid per revolution which is pumped into the delivery port. The displacement D_p of the Digital Displacement pump reduces from the geometric displacement D_{p_geom} with pressure primarily due to the effect of fluid compressibility[5,6], and is varied by the time-averaged fraction F_d of the cylinders which are enabled in a sequence generated by the Pump Controller:

(1) $$D_p = (D_{p\_geom} - P \cdot k_p) \cdot F_d$$

The flow displaced by the pump Q_p enters the high pressure section of the hydraulic circuit

(2) $$Q_p = D_p \cdot \omega_p$$

The flow absorbed by the motor Q_m is higher than expected from the geometric displacement due to leakage and compressibility effects, which are included within the volumetric efficiency term η_{vol_m}

(3) $$Q_m = \frac{D_m \cdot \omega_m}{\eta_{vol\_m}}$$

The difference between pump flow in, and motor flow out of the circuit, accumulates in the fluid compliance of the high pressure section of the circuit. This compliance is not a discrete component but a model of the effect of bulk modulus and hose volumetric elastic expansion:

(4) $$Q_c = Q_p - Q_m$$

The pressure is proportional to the volume accumulated in the compliance:

(5) $$P = k_c \cdot \int Q_c \quad where \quad 0 < P < P_{PRV}$$

The torque generated by the motor τ_m is reduced from ideal according to the mechanical efficiency:

(6) $$\tau_m = D_m \cdot P \cdot \eta_{mech\_m}$$

The energy losses in the pump are represented by the overall efficiency, which increases the load exerted by the pump over the output energy

(7) $$\tau_p = D_p \cdot P \,/\, \eta_{total\_p}$$

The aerodynamic load on the rotor is proportional to the square of the rotor angular velocity ω_r, and varies as a function of planar and axial advance ratio:

(8) $$\tau_r = k_r \cdot {\omega_r}^2 \cdot K_\tau(\mu_x, \mu_y)$$

Each independently controlled rotor is provided with a group of pump cylinders with a separate high pressure output, called a “pumplet”, and the total torque exerted by the pump on the gearbox output shaft is the sum of the torque of the pumplets:

(9) $$\tau_{p\_total} = \sum_1^n \tau_p[n]$$

The gearbox links the torque and speed according to the gear ratio:

(10) $$\tau_g = \tau_{p\_total}/k_g$$

(11) $$\omega_p = \omega_e \cdot k_g$$

The engine generates torque as a function of its speed, the throttle angle set by the controller, and time constant effects:

(12) $$\tau_e = f(\omega_e, \theta, t)$$

The engine is modelled as an inertia acted on by the engine torque, and the gearbox load:

(13) $$\omega_e = \frac{1}{I_e}\int (\tau_e - \tau_g)$$

The rotor is modelled as an inertia acted on by the motor torque, and the rotor aerodynamic load:

(14) $$\omega_r = \frac{1}{I_r}\int (\tau_m - \tau_r)$$

For rotor analysis, the ideal induced velocity is calculated from thrust T, density ρ and rotor area A

(15) $$v_{ii} = \sqrt{\frac{T}{2\rho A}}$$

The ideal rotor power is:

(16) $$Power_{ideal} = v_{ii} \cdot T$$

The actual input rotor power is:

(17) $$Power_{actual} = \tau_r \cdot \omega_r$$

The rotor's figure of merit can then be calculated:

(18) $$\mathrm{FOM} = \frac{Power_{ideal}}{Power_{actual}}$$

4. SIMULATION MODEL

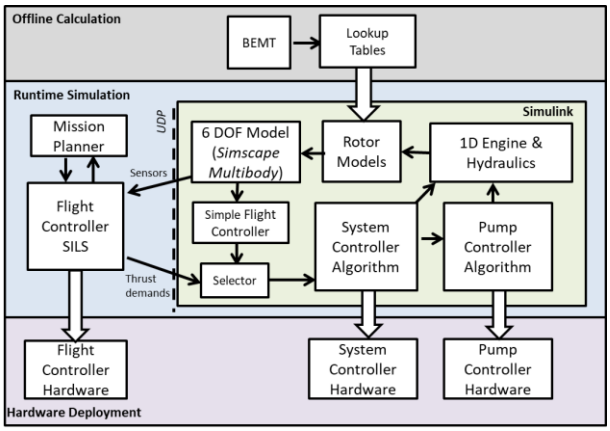

Figure 6: Overall simulation scheme

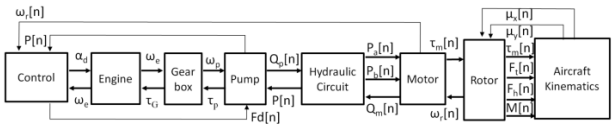

Figure 7: Structure of 1-dimensional propulsion system simulation model

Full details of the simulation model (Figure 6) and associated control system were given in a previous paper[2]. Briefly, the model comprises:

- A 1-D physical model of the coupled engine, pump, hydraulic circuit and motors (Figure 7)
- A rotor model, based on blade element momentum theory, implemented as a lookup-table which returns thrust, torque, h-force and roll moment as a function of axial and tangential advance ratio.
- A 6DOF kinematic model, where the aircraft is treated as a rigid body subject to the forces of gravity, ground contact, drag, and the outputs of the rotor model.
- A system controller, which stabilizes engine speed by varying the throttle, and which stabilizes the rotor speeds according to commands received from a flight controller
- A flight controller, selectable between a simple PID form, and a software-in-the-loop connection to the Ardupilot flight control software.

5. EXPERIMENTAL DEVELOPMENT TO DATE

5.1. Single-axis test rigs

Two test rigs have been built comprising an arm pivoted to allow the vertical motion of a single rotor driven by a hydraulic motor, supplied by a Digital Displacement pump, driven by an electric motor.

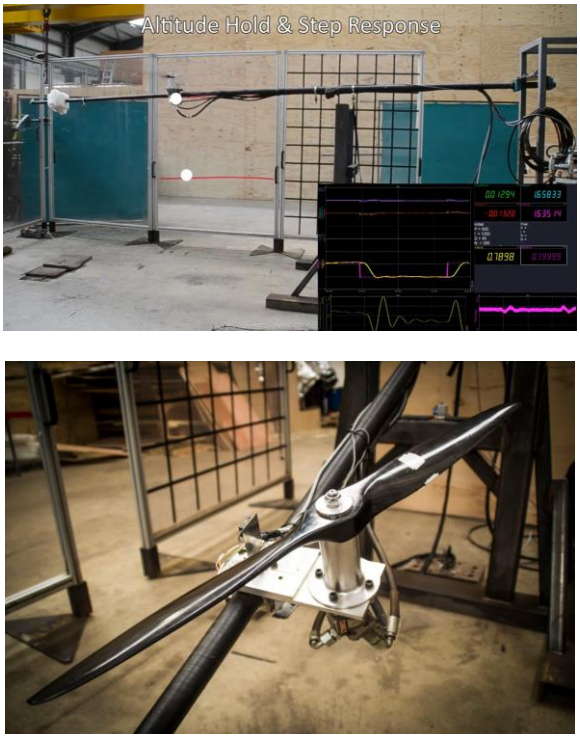

Figure 8 (top) Phase one single axis test rig and time domain response result (bottom) detail of motor and prop

The Phase One test rig was at small scale, up to 10kW. It successfully demonstrated stable hovering flight and rejection of disturbances, and conversely that unstable hover and attitude control is the result of undesirable properties of conventional hydraulic systems such as hysteresis. A video is available[10].

Figure 9 : Phase Two test rig lifting 85kg; the pump is in the foreground on the left.

The Phase Two test rig was at full scale for the H380, including an 18cc hydraulic motor and 1.6m propeller. It successfully demonstrated stable hovering with 85kg of gravitational load. A video is available[11]

6. GROUND-BASED TEST RIG

Figure 10: Ground-based test rig

In Summer 2021, a test cell has been constructed at the Flowcopter facility in Edinburgh, UK. It has interior dimensions L=4.78m, W=4.62m, H=2.25m.

The test frame is built from welded aluminium alloy tubing of 1.5” diameter x 10SWG and has a mass of 45kg.

Mounted on the frame, is a 22kW electric induction motor, powered by a variable-frequency inverter. This takes the place of the combustion engine for initial experimental work. The motor drives the DDP096 Digital Displacement pump. Each of the four high-pressure outlets of the pump supplies a Hydroleduc M12 hydraulic motor, which drive the rotors.

The hydraulic circuit consists of ½” flexible hose of working pressure rating 415 bar, arranged in an open circuit with a low-pressure reservoir boosted by a bladder accumulator precharged with compressed air at approximately 2 bar. Filtration for these tests is by full-flow return line filter, although smaller and lighter off-line filtration is intended for the flight tests. There was no oil cooler; cooling was entirely passive from the system components themselves.

This frame is supported by 4 x 300kg load cells. Further instrumentation is 4 x 600 bar pressure transducers, and 4 x 30ppr encoders for hydraulic motor speeds. Data acquisition is by Dewesoft DEWE-43, with 24 bit ADCs, digital inputs with 100MHz counter/timer, and sychronised CAN message acquisition.

For the tests described herein, the rotors used were E-prop model R-1300, with 1.5m diameter, 2 blades, and ground-adjustable pitch. A table of chord and pitch angle in the nominal (un-pitched) condition is shown in Figure 22: Data table for E-prop R1300 Appendix, Figure 22.

The dimensions of the frame and test cell are shown in Figure 11 and Figure 12 below:

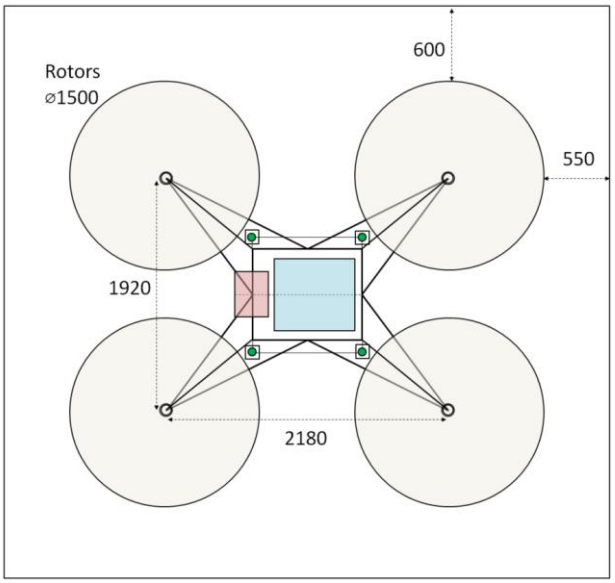

Figure 11: Plan view of the test frame and cell

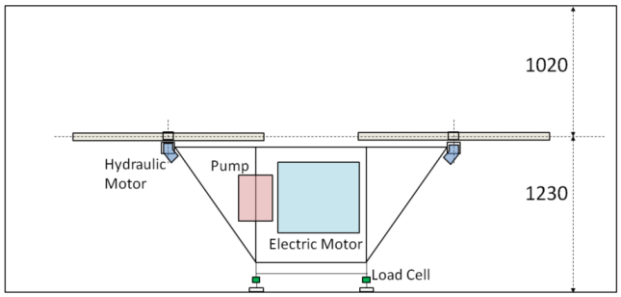

Figure 12: Side view of the test frame and cell

A video of the operation of the ground based test rig is available[12].

7. STATIC ROTOR TESTS

7.1. Thrust and Torque vs Speed

The first set of tests aimed to characterise the rotor thrust and torque as a function of motor speed.

The pump ran at 1800rpm and the speed of the rotor was varied slowly by changing the pump displacement. Thrust was measured by summing the load cell signals in software and subtracting from the static load. Torque was determined from the pressure using 6 and assuming motor mechanical efficiency of 0.94, matching manufacturer data.

The predicted thrust and torque vs rotor speed was calculated from the rotor manufacturer's data[9] for the pitch setting.

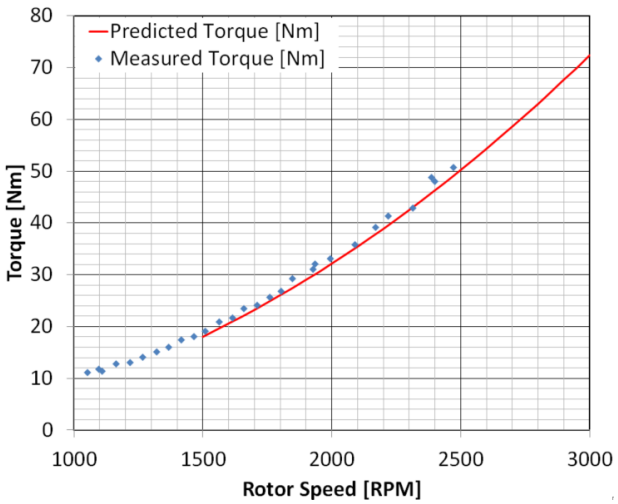

Figure 13: Rotor torque vs speed

The measured rotor torque closely followed the predicted value.

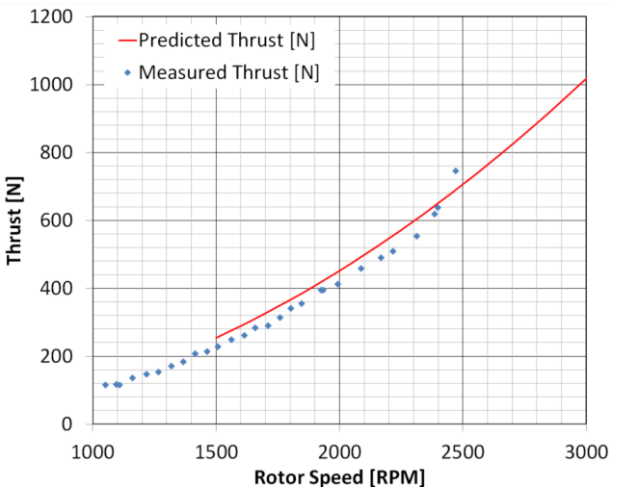

Figure 14: Rotor thrust vs speed

The measured thrust was around 5% lower than predicted across most of the speed range, which indicates that the Figure of Merit is lower than expected.

7.2. Figure of Merit

To calculate Figure of Merit for the rotor, 16, 17 and 18 were used. The density was calculated as 1.148 kg/m3, using the 1976 Standard Atmoshere[14], given the altitude of the site of 146m above sea level and the temperature in the test cell of 30 degrees centigrade.

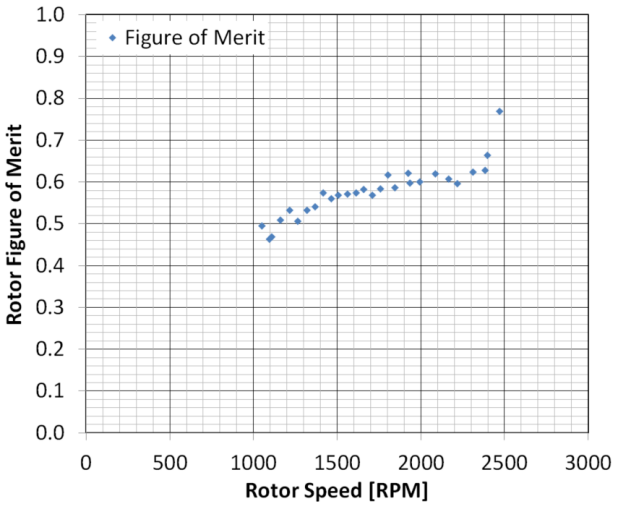

Figure 15: Rotor Figure of Merit vs speed

The measured figure of merit trended towards 0.65 at higher rotor speeds. The figure of merit quoted by the manufacturer was significantly higher at 0.709, but this was assumed to be measured under ideal free-field conditions, without any parasitic drag.

The test cell was not thought ideal for measurement of static thrust due to the proximity of the walls,

ceiling and floor. These effects have been studied by extensively[13] and are tabulated in that reference as scale factors on thrust according to the ratio between the respective distance z to the feature, and the radius R. Given the dimensions in Figure 11 and Figure 12, the ratios for ground, ceiling and wall geometry are 1.64, 1.36 and 1.8 respectively, resulting in negligible error according to this reference.

Another possible explanation for the deviation is the parasitic drag of the test frame. Each of the three test frame arms in the flow field of the rotor is 38mmx750mm, giving an area of obstruction of 0.086m^2 out of a total rotor area of 1.77m^2., around 4.8%, a much more significant effect. This is a more likely explanation for the observed deviation.

7.3. Thrust/Pressure linearity

It is desirable for the control system that the thrust of each motor can be controlled accurately according to the demands of the flight controller. The rotor speed can easily be measured by an encoder in each motor, but the rotor thrust is a function of not only rotor speed but also axial and planar air velocity, and air density. Direct thrust measurement is not practical so it is desirable that motor pressure can be used as a proxy. Therefore the linearity of thrust vs pressure was investigated:

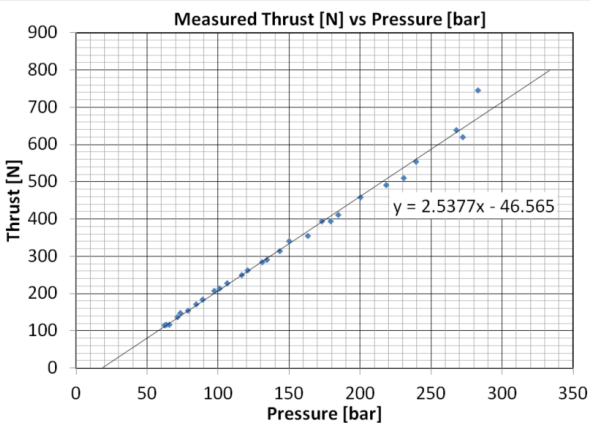

The thrust does indeed seem to be reasonably linear with respect to pressure. The offset of around 20 bar on the pressure axis may be due to friction inside the hydraulic motor.

There is a positive outlook to using the pressure as a proxy for thrust measurement at least in steady state; however it must be remembered that acceleration of rotor inertia also requires motor pressure. Once that is characterised by dynamic tests, it should be possible to compensate for this effect.

8. DYNAMIC ROTOR TESTS

It is fundamental to the control of a quadrotor that the rotor speeds respond quickly to the demands of the flight controller. In the previous paper, the dynamic performance of the H380 was predicted using a 1D model of the engine, hydraulics and rotor coupled to a 6DOF kinematic model. It was desired to validate the 1D model of the hydraulics and rotor in the experiments below, without the complicating factor of the higher-level control systems.

8.1. Test conditions

For these tests, the pump ran at 1000rpm and the speed of the rotor was controlled by changing the pump displacement fraction F_d, in an open loop sequence of steps [0, 0.333, 0.666, 1.000]. Thus, the rotor speed response was determined solely by the physics of the hydraulic circuit, rotor and the low-level delay of the pump displacement control.

The measured and simulated pressure signals were filtered with a 60ms moving average filter to remove high-frequency pulsation and reveal the underlying hydraulic system dynamics.

8.2. Simulation parameters

The following parameters were used in the simulation:

Parameter	Value
Pump capacity [cc/rev]	24
Pump speed	1000
Hydraulic system stiffness [bar/cc]	32
Rotor torque coefficient [Nm@2100rpm]	56.6
Rotor moment of inertia [kgm^2]	0.070

Figure 16: Simulation parameters for dynamic tests

The stiffness was determined by static pump-up test with a locked rotor, according to the method described previously[5]. The rotor torque coefficient matched the steady state value observed for these tests (which were done with a different pitch setting to the static rotor tests). The rotor moment of inertia was not given by the manufacturer and was the only parameter tuned to match the experimental results.

8.3. Results

The complete results for the 30s time series is shown below:

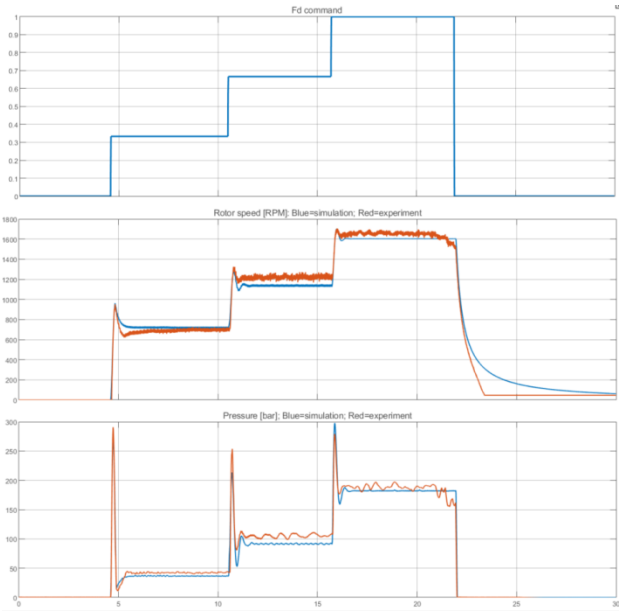

Figure 17: Rotor dynamic complete test (t=0s to t=30s); experimental results [red] compared to simulation [blue]

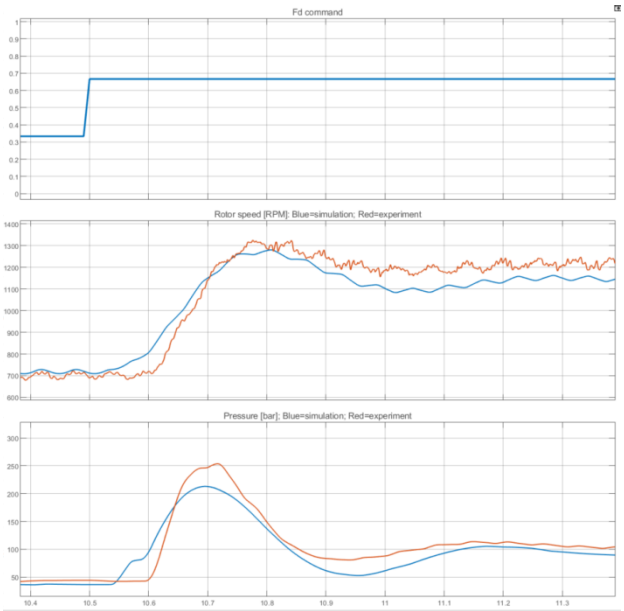

Figure 18: Detail for Fd step from 0.333 to 0.666; t=10.4s to t=11.4s; experimental results [red] compared to simulation [blue]

Each change of pump displacement causes a spike of pressure due to the torque required to accelerate the rotor inertia. The system compliance acts as a spring, which causes a transient overshoot of the rotor speed, in a classical second-order system response.

During the final decay, it is apparent that the experimental rotor speeds decays more quickly below 600rpm than the simulation. This non-linearity is thought to be due to the extra friction in the bearings of the hydraulic motor at low speeds as hydrodynamic effects reduce. This is not an important zone of system operation however so it is not included in the simulation model.

The rotor speed in the experiment reaches the steady value 200ms after the step, with an overshoot of 9.6%, and the simulation gave a similar result. The pressure dynamics also appear similar.

The simulation model seems to give a reasonable match to the measured data. This lends confidence to the predications of dynamic response of the complete H380 system given before[2].

8.4. Potential of more advanced control

To investigate if a more advanced control method could decrease the response time, the Fd sequence was modified such as to have an initial 70ms period of maximum effort (Fd=1) to raise the pressure as quickly as possible, followed by a 40ms period of minimum effort (Fd=0) to lower the pressure quickly to the steady-state value and prevent overshoot. This could be realized as an open-loop model-based control method using the parameters measured in these tests.

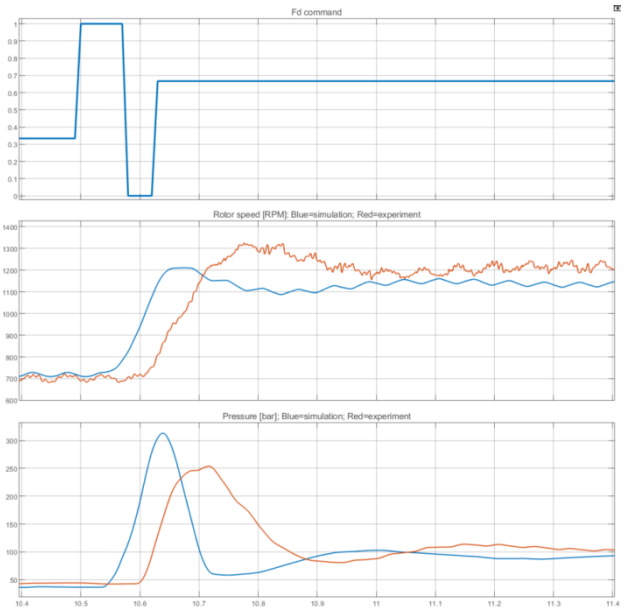

Figure 19: Detail for Fd step from 0.333 to 0.666; t=10.4s to t=11.4s; experimental results [red] compared to simulation with advanced control [blue]

The simulation of the advanced control method shows an improvement of 0-100% step response from 200ms to 130ms. The rate and precision of modulation of pump displacement required is likely only achievable with a Digital Displacement pump.

9. THERMAL TESTS

The final tests were to determine the thermal time constant of the system and the heat loss coefficient.

All four rotors were operated at 1780rpm, such that the electric drive was operated at its power limits. Estimated fluid power was 21.3kW, and pump drive power 22.7kW. Estimated heat loss to the circuit was 3.1kW.

9.1. Steady thermal state

Results of the thermal test is shown below:

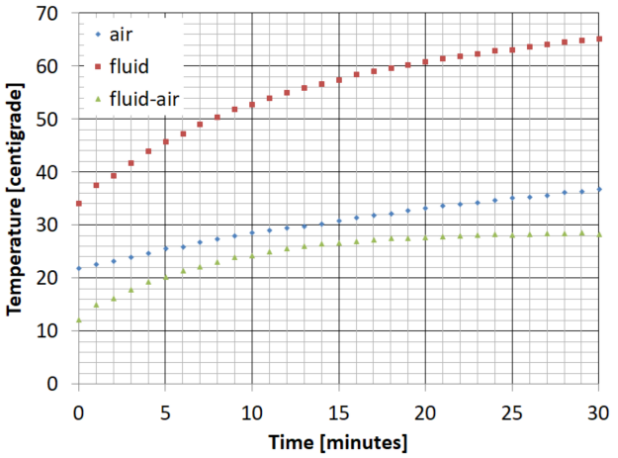

Figure 20: Thermal test results; temperature of air [blue], fluid [red] and delta [green]

The system settled at a steady temperature difference of 28.4 degrees between fluid and air.

The H380 system needs to operate continuously at the continuous power limit of the engine (99kW). This is a factor of 4.4 higher than the power used in this test. Assuming a linear relationship between power and heat loss, and hence temperature difference, would indicate a steady temperature difference of 124 degrees from air to oil. However the maximum allowable oil temperature of the hydraulic components is 90 degrees centigrade, which only allows for 60 degrees temperature difference above an ambient air temperature of 30 C.

It is concluded that the passive cooling of the system components is only half as much as required to keep the system within limits, and a seperate oil cooler will be required.

9.2. Thermal time constant

The exponential decay of the delta temperature was analysed to derive the time constant (Figure 21 below):

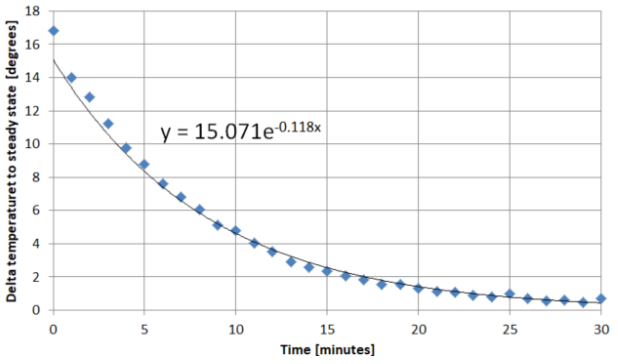

Figure 21: Thermal time constant

The curve fit gives a thermal time constant of 1/0.118 = 8.5 minutes. This means that there is some capacity to absorb transient thermal overloads and indicates that emergency thermal shutdown situations should evolve relatively gradually, with some time to take countermeasures.

Thermal overload is most likely in the hover, (the highest continuous power state expected), and a suitable countermeasure may be to accelerate to the maximum endurance speed (between 24 and 30m/s, depending on weight), where the rotor becomes more efficient, and engine power reduces to about 70% of the hover power[2].

10. CONCLUSIONS

1. The steady state rotor thrust is around 5% than that predicted by manufacturer's data, which seems to be explained by parasitic drag of the test frame.

2. The relationship between thrust and pressure is shown to be substantially linear, so pressure can be used as a proxy for thrust measurement.

3. The predictions of the 1D model match the observed transient behavior, lending confidence to the dynamic results presented previously[2].

4. A more advanced open-loop control method is expected to further decrease the rotor speed step response from 200ms to 130ms.

5. Thermal tests indicate that passive cooling only provides approximately half the cooling power required, so a heat exchanger will be necessary.

6. The thermal time constant of 8.5 minutes seems to be sufficient to take countermeasures in case of overheating during high power conditions such as hover.

11. OUTLOOK

Development is expected to proceed towards flight demonstration in the following ground-based steps:

The Rotax 915is engine will be characterized in both steady state and transient state.

The system controller will be implemented, to both control engine speed and rotor speeds, and interfaced to a flight controller.

The engine will be installed in the test frame in place of the electric motor, and the cooling, electrical and ancilliary systems will be commissioned.

The engine-powered system will be demonstrated on the ground over the full power range using realistic excitation signals from the simulation model, comparing actual thrust to expected thrust from each rotor.

Once ground-based tests are complete, the demonstrator will be flown in tethered indoor tests. A free flight test will be conducted once regulatory permission is granted.

12. REFERENCES

1. Schomann, J “Hybrid-Electric Propulsion Systems for Small Unmanned Aircraft”, Phd thesis, Technical University of Munich, 2014

2. Caldwell N, Rancourt D, McCurry P, Stein U, “Digital Displacement Hydrostatic Transmission for Rotorcraft and Distributed Propulsion”, Paper Number 77-2021-0148, Vertical Flight Society (VFS) 77th Annual Forum & Technology Display, May 10-14, 2021, Virtual, USA.

3. Green M, Macpherson J, Caldwell N, Rampen W, Dexter- The Application of a Digital Displacement Pump to a 16 Tonne Excavator, Proceedings of the 2018 Bath/ASME Symposium on Fluid Power and Motion Control, FPMC2018, September 12-14, 2018, University of Bath, Bath, United Kingdom

4. W. H. S. Rampen and S. H. Salter, “The Digital Displacement Hydraulic Piston Pump,” in Proc. 9th International Symposium on Fluid Power, Oxford, 1990.

5. Caldwell N, Digital Displacement Hydrostatic Transmission Systems, Phd thesis, The University of Edinburgh, 2007, http://www.artemisip.com/published-papers/.

6. Caldwell N, Review of early work on Digital Displacement Hydrostatic Transmission Systems, In BATH/ASME 2018 Symposium on Fluid Power and Motion Control. American Society of Mechanical Engineers.

7. Pellegri M, Green M, Macpherson J, Mackay C, Caldwell N, Applying a multi-service Digital Displacement® pump to an excavator to reduce valve losses, IFK 12th International Fluid Power Conference, October 12-14 2020, Dresden, Germany

8. Caldwell N, “Hydraulic Multi-Rotor Aerial Vehicle”, 2017, Patent application EP18188797.7, US 16/121434, CA301552, CN 201811025060.3

9. E-props Fixed pitched propellers Traction/Torque curves, https://vtol.e-props.fr/curves_fpm.php, accessed March 2021.

10. Flowcopter, Small scale control bandwidth demonstation (video), https://youtu.be/7qV3rbx-_II, accessed March 2021

11. Flowcopter, Full scale single axis test rig lifting 85kg at prop (video), https://youtu.be/MaJM9a-DTms

12. Flowcopter, Flowcopter propeller control (video), https://youtu.be/ubTBGqjlJcg

13. Sanchez-Cuevas, P. J., Martín, V., Heredia, G., & Ollero, A. (2019, November). Aerodynamic Effects in Multirotors Flying Close to Obstacles: Modelling and Mapping. Fourth Iberian Robotics conference (ROBOT 2019), pp. 63-74, Springer, Cham

14. NASA-TM-X-74335, US Standard Atmosphere, 1976, from aerotoolbox.com/atmcalc

APPENDIX 1 – ROTOR DATA

r/R	c/R	Angle [deg]
0	0.0869	20.9
0.2	0.0869	20.9
0.267	0.0897	22.7
0.333	0.0917	21.6
0.4	0.0910	18.3
0.467	0.0917	14.1
0.533	0.0903	11.8
0.6	0.0897	9.4
0.667	0.0862	8.8
0.733	0.0814	8.0
0.8	0.0752	8.0
0.867	0.0690	8.0
0.933	0.0628	9.2
1	0.0566	10.0

Figure 22: Data table for E-prop R1300